Physica E 42 (2010) 2862–2866

Contents lists available at ScienceDirect

Physica E

journal homepage: www.elsevier.com/locate/physe

Hot carrier solar cells: Principles, materials and design

D. König [a,*], K. Casalenuovo [a,b], Y. Takeda [c], G. Conibeer [a], J.F. Guillemoles [d], R. Patterson [a], L.M. Huang [d,a], M.A. Green [a]

[a] ARC Photovoltaics Centre of Excellence, The University of NSW, Sydney, NSW 2052, Australia
[b] Virginia Commonwealth University, Richmond, VA, USA
[c] Toyota Central R & D Labs. Inc., Nagakute, Aichi 480-1192, Japan
[d] IRDEP, UMRCNRS ENSCP EDF R & D, 6 quai Watier, F-78401 Chatou, France

ARTICLE INFO

Article history:
Received 31 August 2009
Received in revised form
18 December 2009
Accepted 22 December 2009
Available online 28 December 2009

Keywords:
Hot carriers
Phonons
Photovoltaics
DFT

ABSTRACT

The concept of hot carrier solar cells is discussed in terms of carrier cooling, conditions of energy- and carrier-selectivity for the energy selective contacts and macroscopic device behaviour. From the findings for hot carrier absorbers, we carried out high accuracy density functional calculations of hydrogen-terminated diatomic molecules, with results used in an infinite diatomic chain model for estimating phononic properties of material candidates. We evaluate phonon confinement as a function of structure size and intentional material mismatch, relating the accompanying constraints in electronic properties to the requirements of hot carrier absorbers. The evaluation of material candidates for hot carrier absorbers and energy selective contacts regarding their phononic, electronic, optical and structural properties provides us with a more detailed description of a practicable hot carrier solar cell.

1. Introduction

Electron–hole pairs generated in conventional solar cells (SCs) lose energy by cooling down from their initial energetic (“hot”) position to the band edges by optical phonon emission. Hot carrier (HC) SCs attempt to minimise this loss by extracting carriers at elevated energies in a narrow range, requiring a substantial delay in carrier cooling in the hot carrier absorber (HCA) and energy selective carrier extraction by an energy selective contact (ESC) [1], see Fig. 1. HCs have to undergo quasi-ballistic carrier transport, allowing for elastic carrier–carrier scattering, for minimum extraction time. This is underlined by recent findings, where the optimum ratio of time constants for HC retention and HC thermalisation is $\tau_{re}/\tau_{th} \approx 1/10$ [2].

2. Hot carrier absorbers (HCAs)

2.1. General carrier cooling dynamics and energy loss mechanisms

Carrier cooling in bulk semiconductors occurs within 10–100 ps, see Fig. 2. We describe the process for electrons; it also applies to holes. Optical generation of carriers is instantaneous, generated carrier populations are a convolution of photon flux and HCA electronic DOS. Electrons have individual energies and do not interact yet apart from spin selection rules. At 10–100 fs, electron–electron interaction sets in by elastic scattering, leading to energy re-normalisation for hot electrons, or to impact ionisation of valence band electrons (Auger generation). Auger-recombination, the reverse process, is no loss mechanism as the energy released re-heats the free electron. Energy re-normalisation leads to a Fermi–Dirac electron population with one high temperature. With no additional phonons generated yet, the lattice is in thermal equilibrium. Electron–optical phonon (Fröhlich) interaction sets in by local electrostatic lattice distortion, forming polarons. Second quantisation of this vibrational lattice excitation yields optical phonons, thus electron energy loss by optical phonon emission. Optical phonons decay further into acoustic phonons, but can also re-heat free electrons, see Figs. 2 and 9. Optical phonon emission and decay proceed until electrons have thermalised. Acoustic phonons heat the lattice, affecting quasi-ballistic carrier transport. Free carriers yield to direct (radiative) and indirect (Hall–Shockley–Read—HSR) recombination. Photons generated by the former can be re-absorbed by ground state transitions or by free carrier re-absorption. HSR recombination is at least three orders of magnitude slower than electron cooling.

2.2. Losses by optical phonon emission

Minimising the energy quantum $\hbar\omega_0$ of optical phonons delays carrier cooling. Optical phonon emission occurs in a short,

* Corresponding author.
E-mail address: dirk.koenig@unsw.edu.au (D. König).

1386-9477/$ - see front matter
doi:10.1016/j.physe.2009.12.032

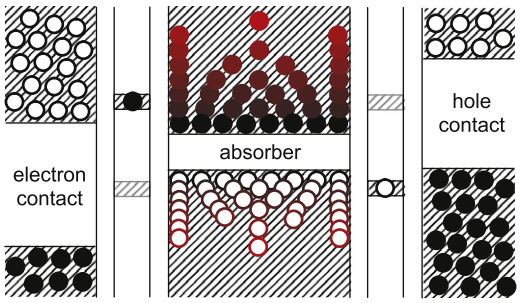

Fig. 1. Schematic of HC-SC. Hot carriers in HCA get extracted in small energy range via ESC into macroscopic contact. Output voltage given by difference in chemical potential of extracted carriers minus carrier cooling during extraction.

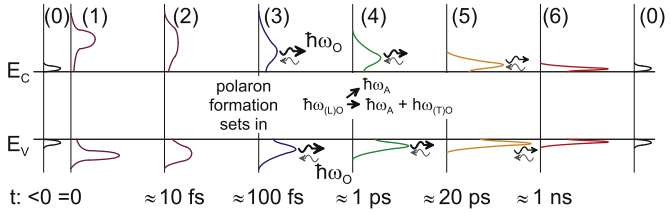

Fig. 2. Carrier cooling kinetics in bulk semiconductor: Thermal equilibrium (0); immediately after optical generation (1); carrier–carrier scattering, impact ionisation, re-normalisation of carrier energies, Fermi–Dirac statistics (2); optical phonon emission (re-absorption) (3); decay of optical into acoustic phonons (4); further phonon emission (5), to thermal equilibrium, onset of carrier recombination (6).

yet finite time. With lower $\hbar\omega_O$, electrons have to emit more optical phonons for a certain energy loss. A minimum $\hbar\omega_O$ can be reached by binary compounds with a larger mass for the lighter atom as evident from the $\omega(\mathbf{k})$ dispersion of a 1d diatomic chain,

$$\omega_{\pm} = \sqrt{\gamma\left[\frac{1}{\mu_m} \pm \sqrt{\left(\frac{1}{\mu_m}\right)^2 - \frac{4}{m_b m_s}\sin^2(\mathbf{ak}/2)}\right]}$$

$$\text{with reduced eff. mass } \mu_m = \frac{m_b m_s}{m_b + m_s}, \qquad (1)$$

where ω_+ and ω_- (rad^{-1} s^{-1}), γ (N m^{-1}), m_b and m_s (kg), μ_m (kg) and $\mathbf{a}$ (m) describe the optical and acoustic phonon branch, the force constant of the vibrating bond, masses of the heavy and light atoms, reduced mass of the oscillating system and the length of the 1d unit cell—here two bond lengths for a diatomic chain—respectively.

Excited electrons form polarons with radii of 20–90 Å for most solids [3]. Fröhlich interaction describes electron–optical phonon coupling. In solids with large dielectric constant ε_{rel} and low electron effective mass m^n_{eff}, the Fröhlich interaction constant $\alpha_{Frö}$ is small [3]. A low m^n_{eff} decreases electron momentum, leading to smaller atomic elongations. It also enhances hot carrier generation as the free electron energy is $E(e^-) = (\hbar\mathbf{k})^2/2m^n_{eff}$. Electrostatic screening by a large ε_{rel} decreases the polaron radius and thus the number of atoms affected. For the same reason, co-valent solids are attractive as the dipole moment of the atomic bonds is very small.

2.3. Phonon decay mechanisms

An optical phonon with $\mathbf{k}_0$ decays into two acoustic phonons by Klemens-decay (KD) [4]. Acoustic phonon states must fulfil momentum and energy conservation, $\mathbf{k}_1 + \mathbf{k}_2 = \mathbf{k}_0$ and $\hbar\omega_O(\mathbf{k}_0) = \hbar\omega_A(\mathbf{k}_1) + \hbar\omega_A(\mathbf{k}_2)$. A phononic band gap exceeding the maximum energy of acoustic phonons, $E_{gap}(\hbar\omega) > \max(\hbar\omega_A)$, prevents KD and is achieved for $m_b > 4m_s$, see Eq. (1). Space group symmetry changes the degeneracy of phononic branches by their dispersion. For solids with high symmetry group, e.g. face-centred cubic, a decreased dispersion of phonon branches opens up the phonon gap.

Ridley described an optical phonon decay into an acoustic phonon and another optical phonon with lower energy [5]. Energy- and $\mathbf{k}$-conservation render the Ridley-decay (RD) to proceed like $\hbar\omega_{LO}(\mathbf{k}_0) \rightarrow \hbar\omega_{TO}(\mathbf{k}_0 + \mathbf{k}) + \hbar\omega_{LA}(\mathbf{k}_0 - \mathbf{k})$ [6]. RD could also proceed from TO phonons, but these have a lower energy than LO modes, leading to the reverse process, a LA and TO phonon superimposing to a LO phonon. Unlike KD, RD is not prevented by a large phononic gap due to the energetic difference of the optical and acoustic phonon decay states. RD can be suppressed by breaking energy- or $\mathbf{k}$-conservation, originating from different first derivatives $\partial\omega/\partial\mathbf{k}$ for optical and acoustic dispersion branches over the $\mathbf{k}$-range of initial and decay states. A low $\partial\omega_O/\partial\mathbf{k}$ results in a low optical phonon dispersion $\hbar\Delta\omega_O$ with little energy lost and can be achieved by a maximum difference of m_b and m_s, see Eq. (1). Solids with high space group symmetry have a high degeneracy of the optical branches, limiting RD as fewer optical branches exist into which the LO mode could decay. KD and RD mechanisms are shown in Fig. 3.

2.4. Phononic properties of HCA candidates

Phononic properties discussed above can be estimated by the 1d diatomic chain model with input from density functional theory (DFT) calculations of vibrational spectra using hydrogen (H) terminated diatomic molecules like H_3SiGeH_3 or H_2BiSH_3. The molecules constitute elements of various binary compound candidates for HCAs.

DFT computations were carried out with the software suite GAUSSIAN03 [7]. Approximants were optimised with the B3LYP hybrid functional [8] until forces acting on all atoms were below 408 μeV/Å, followed by a frequency analysis. Core electrons were treated by the effective core potential included in the augmented correlation-consistent polarised valence triple zeta (aug-cc-pVTZ-PP) molecular orbital (MO) basis set describing states of bonding valence and anti-bonding MOs [9].

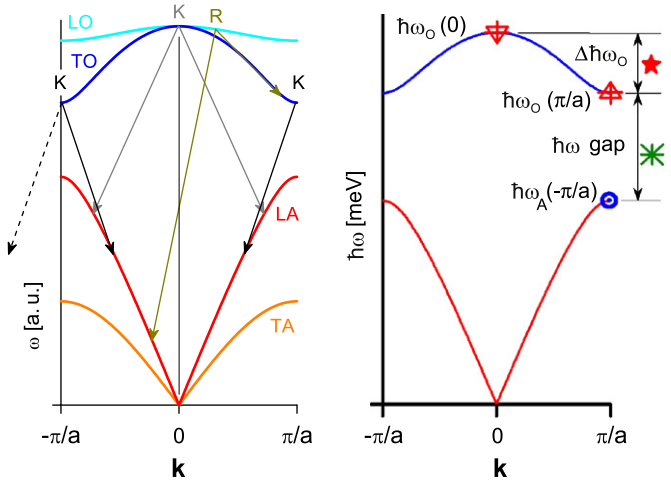

Fig. 3. $\hbar\omega(\mathbf{k})$ dispersion of quasi-1d diatomic chain (left), allowing elongations orthogonal to diatomic chain. KD and RD shown by arrows. KD at BZ edge due to *umklapp*-process (dashed arrow). $\hbar\omega(\mathbf{k})$ dispersion of 1d diatomic chain (right), allowing longitudinal modes only [6]. Important parameters: max. acoustic phonon energy $\hbar\omega_A(\pi/\mathbf{a})$, min. optical phonon energy $\hbar\omega_O(\pi/\mathbf{a})$, max. optical phonon energy $\hbar\omega_A(\mathbf{0})$, dispersion of optical branch $\Delta\hbar\omega_O$, phononic band gap $\hbar\omega$ gap. Symbols refer to bottom graph in Fig. 4.

The LO vibrational mode obtained from DFT is corrected for the H masses, with its wave number ν_{LO} fed as ω_{LO} into the 1d model. As both central atoms of the molecule oscillate and the oscillation is self-contained therein (standing vibration), we get $\mathbf{k}(\omega_{LO}) = \mathbf{0}$ [6], whereby we can calculate γ and the entire 1d phonon dispersion. Comparing ν_{LO} with experimental data of weak polar compounds like AlSb shows close agreement, see top graph of Fig. 4. Deviations from experiment increase with the polarity of atomic bonds as for InN. A more precise description of vibrational properties would require several shells of next-neighbour atoms for electrostatic interaction. Space group symmetry cannot be evaluated, leading to deviations especially for compounds with multiple crystal phases like SiC. GaAs, SiC and SiGe are included for comparison.

The bottom graph of Fig. 4 shows the 1d model results. Borides and nitrides are very hard materials, reflected in a large γ (rigid bonds). HCA materials should have a phononic band gap of $E_{gap}(\hbar\omega) > \max(\hbar\omega_A)$, a low $\hbar\Delta\omega_O$, $\hbar\omega_O$ and m^n_{eff}, and a large ε_{rel}, the latter two for a small $\alpha_{Frö}$ (not shown). The most attractive HCA materials are compounds of heavier light elements with bismuth (Bi) like Bi_2S_3 or AlBi. These materials can be processed at low temperatures like Bi_2S_3 at 250 °C [10]. Bi is the heaviest non-radioactive element and has a low electronegativity for a group V element, with Bi compounds like BBi or BiP being nearly co-valent. Other attractive materials are SiSn, BSb and InP. Group III nitrides have a polar bond, yielding a higher electron–phonon interaction (Fröhlich constant) and hence are no good material candidates.

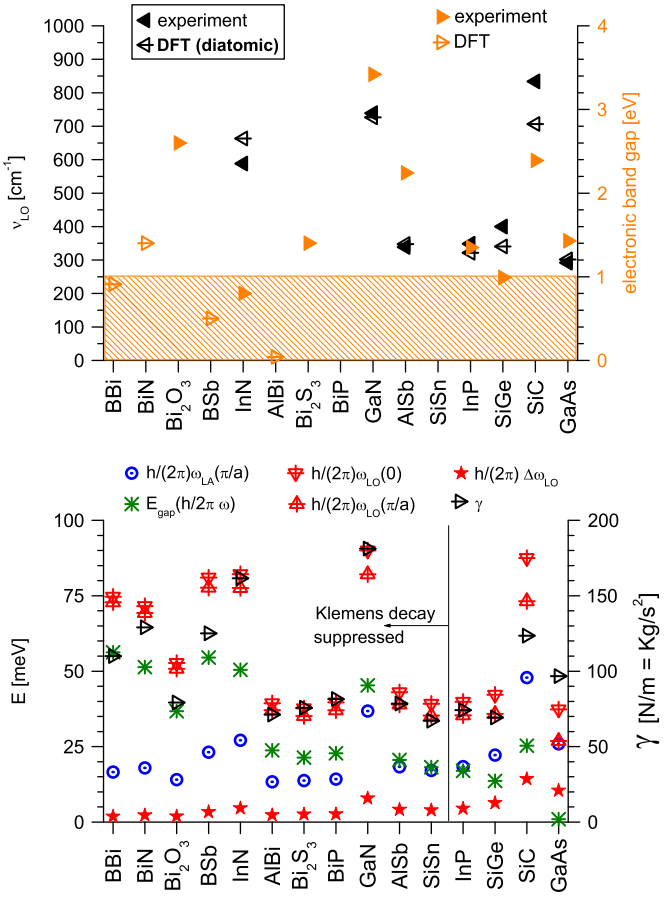

Fig. 4. LO mode wave numbers obtained experimentally [12] and by our model (top). Values for electronic band gaps from literature [12,13] refer to right scale. Range of electronic band gaps for HCAs shown in shaded orange/grey. Phononic parameters obtained from our model (bottom); symbols explained in right graph of Fig. 3. Force constants γ of compounds refer to right scale. (For interpretation of the references to colour in this figure legend, the reader is referred to the web version of this article.)

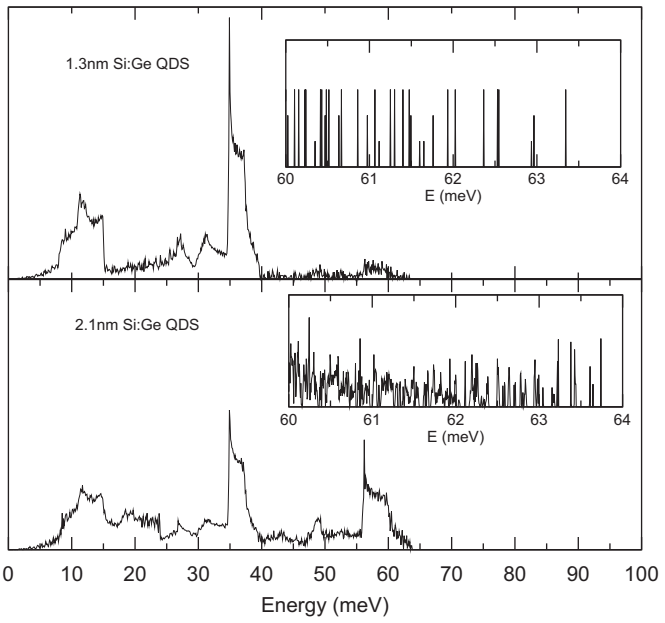

Fig. 5. Phononic DOS of Si NCs in a Ge matrix as a function of phonon energy [15]. Very small minigaps exist in the energy range of optical phonons for 13 Å Si NCs (top), converging to quasi-continuum for 21 Å Si NCs (bottom).

2.5. *Phonon confinement*

Nano-structures can delay carrier cooling as shown by Nozik [11], with several effects contributing. We evaluate these for carrier cooling delay.

The length of the vibrational wave packet forming an optical phonon is very small. This oscillation length is the characteristic phonon extension (CPE) [6]. The minimum CPE is given by a standing wave with a zero phonon group velocity ($\mathbf{v}_{gr} = \mathbf{0}$), leading to a maximum number of phonon modes per unit length, hence a maximum DOS($\hbar\omega$). The CPE increases with $\mathbf{v}_{gr}$ up to several lattice planes, which decreases the number of phonon modes per unit length and thus DOS($\hbar\omega$). A minimum CPE yields a maximum DOS($\hbar\omega$), making phononic confinement most effective for structures consisting of two lattice planes—a binary compound. For $2n$ lattice planes, we get n mini gaps. Their sum stays constant, decreasing the energy per minigap for an increasing number of lattice planes. Minigaps get more localised in $\mathbf{k}$-space with the number of lattice planes, resulting in a continuous DOS($\hbar\omega$) over most $\mathbf{k}$. Minigaps can slow down phonon decay if they block $\omega_O(\mathbf{k})$- regions relevant for phonon decay. The CPE is small as compared to the exciton radius $\mathbf{a}_{exc}$ typically in the range of 40–100 Å for materials of interest [3]. Fig. 5 shows the effect of a phononic super lattice (SL) on the DOS($\hbar\omega$) calculated by DFT and gives an impression on the structure size. A force constant model yielded similar results [14].

Phonon confinement and carrier quantum confinement occur at different structure sizes, with no or very little overlap. For a HC population, at least a quasi-continuous carrier DOS is required [6]. Hot carriers with a Fermi–Dirac distribution do not exist in a discrete carrier DOS. While SLs delay carrier cooling [11], it remains to be shown to what extent HCAs benefit from phonon confinement *by size effects* in analogy to electronic quantum confinement.

The other cause for slowed carrier cooling in nano-structure (NS) HCAs is phonon confinement *by material effects*. Phonons are

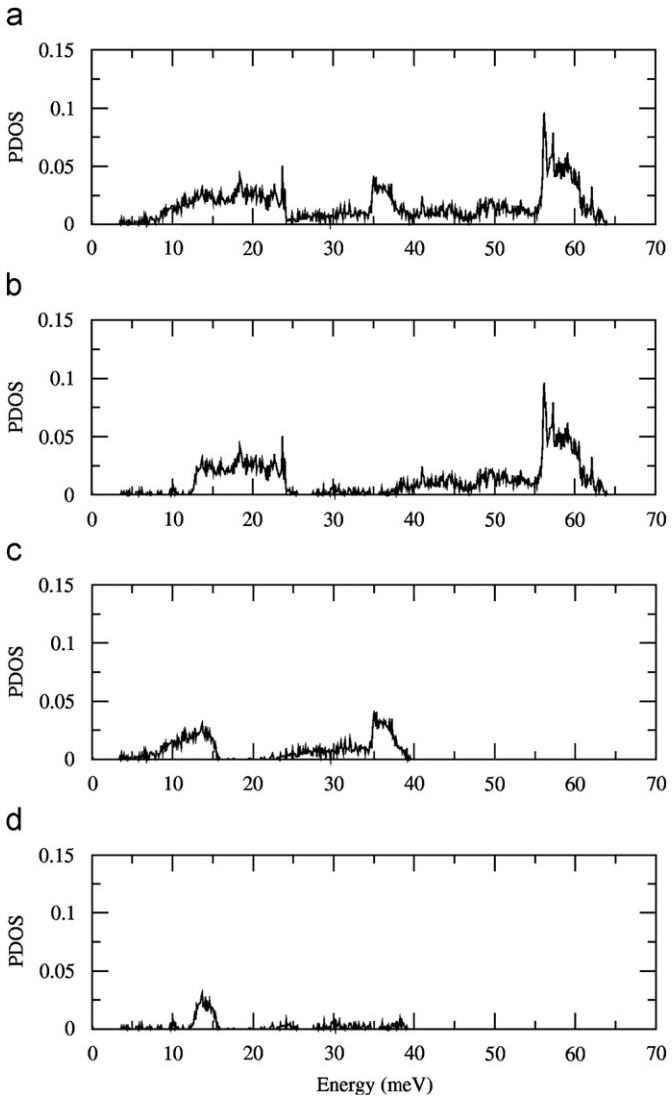

Fig. 6. Total phononic DOS of Si NDs in Ge matrix as a function of energy (a), partial DOS of Si NDs (b) and Ge matrix (c), shared DOS between Si NDs and Ge matrix (d) [15]. High energy Si optical modes cannot propagate into Ge.

reflected back into the HCA by a vibrationally mismatched matrix material, see Fig. 6. There is no phononic DOS in Ge allowing Si optical modes above 40 meV to propagate from the Si nano dot (ND). This is a powerful means of phonon confinement, with no strong dependence on NS size.

3. Energy selective contacts (ESCs)

ESCs consist of a tunnel barrier with resonant level (energy selective level—ESL) of width ΔE_{ESL}. Energy selectivity is given by ESL, beyond which all electrons are reflected back into the HCA. Carriers cool with very low entropy production during extraction, losing some energy at the macroscopic contact in order to avoid back-diffusion, see Fig. 7.

ESLs with sharp transitions minimise cooling during extraction. Highest energy selectivities are obtained by quantum dots (QDs) or atomic impurities, see Fig. 7. Quantum wires and wells show stronger carrier cooling by continuous electronic DOS in lateral ESC direction [16]. ESLs formed by atomic impurities do not suffer from size deviations like QDs. Iso-valent impurities form a neutral ESL miniband with low electron exchange-correlation interaction. Such

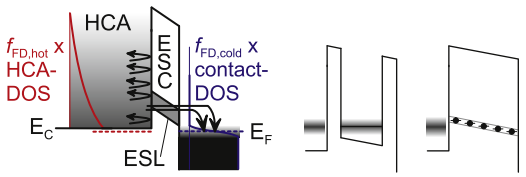

Fig. 7. ESC with current flow: working principle (left), ESL formation by QD array (centre) or impurities (right). Graded bars show ESL blurring, occurring by size deviation in QD arrays or by diffusion field tilting of impurity miniband.

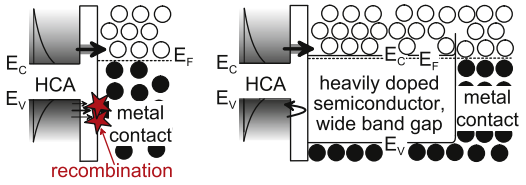

Fig. 8. Metal contacts at ESC destroy carrier selectivity by recombinative tunnelling of minorities [holes] (left). Spacer layer of heavily [n] doped semiconductor removes allowed states for minorities, reflecting them back into HCA (right).

an ESL position depends less on its occupancy and is more robust for carrier transport. QDs can have considerable eigenenergy shifts as a function of occupancy. Coulomb blockade effects may prohibit resonant transport altogether.

Highest HC-SC efficiencies (Carnot ~) result from $\Delta E_{ESL} \to 0$ at vanishing energy (carrier) flux. A low ESC barrier without ESL represents a thermoelectric contact with high carrier flux and massive carrier cooling, thus much lower efficiency. The optimum is a compromise given by ΔE_{ESL} matching the current density $\mathbf{j} = -qd_{HCA}(G_{opt} - R_{HSR})$, with q, d_{HCA}, G_{opt}, R_{HSR} being elementary charge, HCA thickness, optical generation rate and HSR recombination rate, respectively.

ESCs must accomplish carrier selectivities realised by highly doped regions in conventional SCs because dopants in a HCA accelerate cooling by acting as scattering centres. The ESC barrier alone cannot prevent recombinative minority carrier tunnelling into metal contact. A wide band gap semiconductor highly doped with the extracted carrier type as majorities works as buffer layer and removes the states into which minorities can tunnel, see Fig. 8.

4. Working principle and device behaviour

The processes in a HC-SC providing a steady-state HC population with HC extraction into macroscopic contacts are shown in Fig. 9. Carrier selectivities integrated into ESCs are carrier valves like p^+ and n^+ regions in conventional SCs. Carrier diffusion by quasi-ballistic transport thereby governs device behaviour, rendering the qualitative HC-SC device characteristics to be that of a conventional solar cell, see Fig. 10. Ultrafast quasi-ballistic carrier extraction with $\tau_{re} \approx 100$ ps leads to HCA carrier densities of 10^{12} to 10^{15} cm^{-3} for a photon flux of 1–1000 Suns [2], with complete carrier extraction. HSR recombination is thus a marginal loss confirmed by high HC-SC efficiencies [1,2]. A photon flux of 1000 Suns, AM 1.5, yielded conversion efficiencies of 55%, assuming feasible, yet unachieved carrier thermalisation times of $\tau_{th} = 1$ ns [2].

5. Conclusion

We discussed concepts and materials of HCAs, ESCs and HC-SC devices. BBi, BiN, AlBi, BiP, Bi_2S_3, SiSn, BSb and InP are good HCA material candidates. Phonon confinement in HCAs by size effects

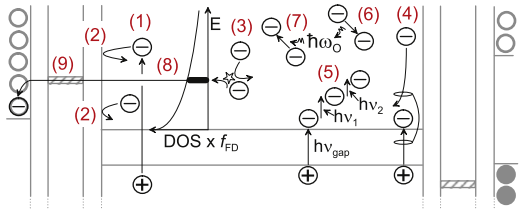

Fig. 9. HC-SC with mechanisms changing electron energy: hot exciton generation (1), reflected electrons at ESC (2), energy re-normalisation by electron–electron-scattering, refilling DOS subject to carrier extraction (3), impact ionisation (4), free electron re-absorption of sub-bandgap photons (5), optical phonon emission (6) and re-absorption (7), quasi-ballistic transport (8), energy selective tunnelling from HCA (9).

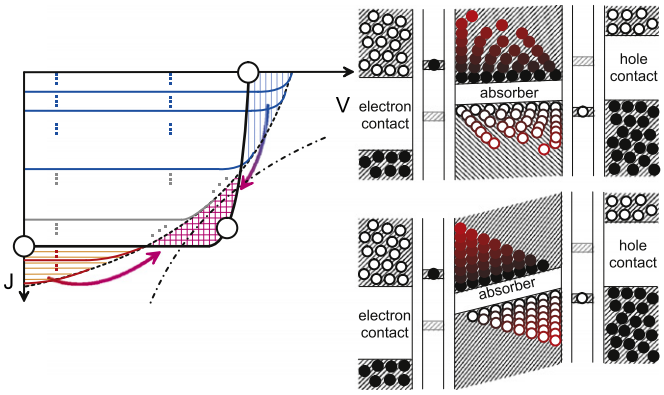

Fig. 10. Qualitative JV-behaviour of HC-SC [left]. Single-particle tandem cells in parallel describe all hot carrier generation processes by photons (dashed black line). Elastic carrier–carrier-scattering moves cold electrons from low-voltage region and very hot electrons from high voltage region on top of carrier density in intermediate energy range, pushing power flux (maximum power point—MPP) and efficiency beyond thermodynamic limit (dot-dashed black line) for single junction SC. Band diagrams for MPP [top right] and short circuit [bottom right]. Open circuit case shown in Fig. 1.

occurs in structures too small to meet required electronic properties. Confinement by phononic material mismatch in bigger structures with relaxed periodicity can meet both, electronic and phononic HCA properties. ESCs must be energy- and carrier-selective as HCA doping promotes carrier cooling. The latter ESC property renders HC-SCs to behave qualitatively like conventional solar cells. ESLs formed by iso-valent impurities are more robust in energy than QDs arrays. HSR recombination losses were found to be marginal, which is supported by very high projected conversion efficiencies.

Acknowledgement

Financial support by the Australian Research Council Centre of Excellence scheme and by the Global Energy Climate Project (GCEP) is acknowledged.

References

[1] R.T. Ross, A. Nozik, J. Appl. Phys. 53 (1982) 3813;
P. Würfel, Sol. Energy Mater. Sol. Cel. 46 (1997) 43;
M.A. Green, Third Generation Solar Cells, Springer, Berlin, 2003;
G. Conibeer, N. Ekins-Daukes, J.-F. Guillemoles, et al., Thin Solid Films 516 (2008) 6948;
G.J. Conibeer, D. König, M.A. Green, et al., Sol. Energy Mater. Sol. Cel. 93 (2009) 713.
[2] Y. Takeda, T. Ito, T. Motohiro, et al., J. Appl. Phys. 105 (2009) 074905.
[3] K.W. Böer, Survey of Semiconductor Physics, vol. 1, Van Nostrand Reinhold, New York, 1990.
[4] P.G. Klemens, Phys. Rev. 148 (1966) 845.
[5] B.K. Ridley, Phys. Rev. B 39 (1989) 5282.
[6] D. König, Nanotechnology for Photovoltaics, in: L. Tsakalakos (Ed.), CRC Press, Boca Raton, FL, January 2010 (Chapter 3).
[7] GAUSSIAN03, Revision D 0.1, Gaussian, Inc., Wallingford CT, 2004, see 〈http://www.gaussian.com/citation.htm〉.
[8] D. Becke, Phys. Rev. A 38 (1988) 3098;
C. Lee, W. Yang, R.G. Parr, Phys. Rev. B 37 (1988) 785.
[9] B. Metz, H. Stoll, M. Dolg, J. Chem. Phys. 113 (2000) 2563;
K.A. Peterson, J. Chem. Phys. 119 (2003) 11099;
K.A. Peterson, D. Figgen, E. Goll, et al., J. Chem. Phys. 119 (2003) 11113.
[10] B. Pejova, I. Grozdanov, Mater. Chem. Phys. 99 (2006) 39.
[11] A.J. Nozik, Ann. Rev. Phys. Chem. 52 (2001) 193.
[12] S. Adachi, Handbook on Physical Properties of Semiconductors, vols. 1 and 2, Kluwer, Boston, 2004;
E. Kasper, K. Lyutovich (Eds.), Properties of Silicon Germanium and SiGe: Carbon, INSPEC, London, 2000.
[13] V.Y. Davydov, A.A. Klochikhin, V.V. Emtsev, et al., Phys. Stat. Sol. B 230 (2002) R4;
V.V. Killedar, C.H. Bhosale, C.D. Lokhande, Tr. J. Phys. 22 (1998) 825;
S.Q. Wang, H.Q. Ye, Phys. Rev. B 66 (2002) 235111;
H. Meradji, S. Drablia, S. Ghemid, et al., Phys. Stat. Sol. B 241 (2004) 2881.
[14] R. Patterson, M. Kirkengen, B. Puthen Veettil, et al., Phonon lifetimes in quantum dot superlattices, talk B54, E-MRS Meeting, Strasbourg, France, 8–12 June 2009, Sol. Energy Mater. Sol. Cel., in review process.
[15] L.M. Huang, J. Zafran, A. Le Bris, et al., in: Proceedings of the 23. E-PVSEC, Valencia, Spain, 1–5 September 2008, pp. 689–691;
G. Conibeer, R. Patterson, L.M. Huang, et al., in: Proceedings of the 23. E-PVSEC, Valencia, Spain, 1–5 September 2008, pp. 156–162.
[16] M.F. O'Dwyer, R.A. Lewis, C. Zhang, et al., Phys. Rev. B 72 (2005) 205330.